Materials Today Bio 32 (2025) 101677

Contents lists available at ScienceDirect

Materials Today Bio

journal homepage: www.journals.elsevier.com/materials-today-bio

Porcine pericardium crosslinked with POSS-PEG-CHO possesses weakened immunogenicity and anti-calcification property

Xiaobo Yu [a,b,c,1], Jingli Ding [d,1], Yingjie He [e,1], Shunbo Wei [a,b,c], Xing Chen [a,b,c], Qiujie Luo [a,b,c], Yuqing Zhang [a,b,c], Chen Qian [a,b,c], Jiahui Wang [a,b,c], Mengjie Hu [a,b,c], Xiang Zhang [a,b,c], Cuifen Lu [e,*], Jinping Liu [a,b,c,**], Jianliang Zhou [a,b,c,***]

[a] Department of Cardiovascular Surgery, Zhongnan Hospital, Wuhan University, Wuhan, Hubei Province, 430071, China
[b] Hubei Provincial Engineering Research Center of Minimally Invasive Cardiovascular Surgery, Wuhan, Hubei Province, 430071, China
[c] Wuhan Clinical Research Center for Minimally Invasive Treatment of Structural Heart Disease, Wuhan, Hubei Province, 430071, China
[d] Department of Gastroenterology, Zhongnan Hospital of Wuhan University, Wuhan, Hubei Province, 430071, China
[e] Hubei Key Laboratory for Precision Synthesis of Small Molecule Pharmaceuticals & Ministry-of-Education Key Laboratory for the Synthesis and Application of Organic Functional Molecules, Wuhan, Hubei Province, 430062, China

ARTICLE INFO

Keywords:
Biological heart valve
Crosslinking
Polymer
Calcification
Immunology

ABSTRACT

Valvular heart disease (VHD) poses a thorny problem in cardiovascular diseases. The most effective treatment for VHD is heart valve replacement. Biological heart valve (BHV) is more favored than mechanical heart valve due to the maturity of transcatheter heart valve replacement (THVR) and the absence of the need for lifelong anticoagulant use. However, traditional commercial BHV suffers degeneration within 10–15 years because of calcification caused by the cross-linking reagent, glutaraldehyde. Considering the remarkable properties of POSS, PEG, and the star-like eight-arm structure, we fabricated POSS-PEG-PP, which is a decellularized porcine pericardium (DPP) crosslinked by a star-like eight-arm cross-linker octafunctionalized POSS of benzaldehyde-terminated polyethylene glycol (POSS-PEG-CHO) based on the Schiff's base reaction. POSS-PEG-PP exhibits more intense fiber arrangement and better mechanical properties than GLUT-PP (glutaraldehyde crosslinked DPP). The results also show that the cytocompatibility, endothelialization, and hemocompatibility of POSS-PEG-PP are outstanding in vitro. Subsequently, in vivo assessments demonstrate that POSS-PEG-PP has anti-inflammatory and anti-calcification abilities. Furthermore, RNA sequencing analysis of subcutaneous implants suggests that the intervention of AMPK and IL-17 signaling pathways plays an important role in the inflammatory and immune responses regulation of POSS-PEG-PP. Therefore, POSS-PEG-PP is an excellent substitute material for BHVs and is expected to be clinically transformed.

1. Introduction

Valvular heart disease (VHD) ranks as the third most common cardiovascular condition, only following coronary artery disease and hypertension. Currently, there are no pharmaceutical treatments approved for VHD, and the only curative option is heart valve replacement, which can be performed using either mechanical heart valve (MHV) or biological heart valve (BHV) [1,2]. Recently, BHV has gained preference over MHV because MHV requires lifelong anticoagulant therapy and BHV is more suitable for Transcatheter Heart Valve Replacement (THVR) [3,4]. However, the majority of commercially available BHVs, which are primarily made from glutaraldehyde-crosslinked porcine or bovine pericardium, tend to undergo degenerative changes within 10–15 years due to calcification [5]. The calcification of BHV is primarily attributed to immune responses, thrombosis, and the toxicity of glutaraldehyde [6,7]. Hence, there is a pressing need for innovative

* Corresponding author.
** Corresponding author. Department of Cardiovascular Surgery, Zhongnan Hospital, Wuhan University, Wuhan, Hubei Province, 430071, China.
*** Corresponding author. Department of Cardiovascular Surgery, Zhongnan Hospital, Wuhan University, Wuhan, Hubei Province, 430071, China.
E-mail addresses: lucf@hubu.edu.cn (C. Lu), liujinping@znhospital.cn (J. Liu), zjl20210802@whu.edu.cn (J. Zhou).
[1] Equal contribution.

https://doi.org/10.1016/j.mtbio.2025.101677
Received 23 December 2024; Received in revised form 19 February 2025; Accepted 16 March 2025
Available online 18 March 2025

cross-linking techniques that can endow BHV with reduced immunogenicity, improved cytocompatibility, hemocompatibility, and anti-calcification properties.

Over the past few decades, a variety of methods have been explored to replace glutaraldehyde in the crosslinking process of BHV. These include the use of epoxy compounds [8], polyphenols [9,10], 1-ethyl-3-(3-dimethylaminopropylcarbodiimide hydrochloride/N-hydroxy-succinimide (EDC/NHS) [11], oxidized hyaluronic acid [12] and photo crosslinking techniques [13,14]. Despite the potential benefits of these alternatives, such as reduced cytotoxicity and improved resistance to calcification, none have been implemented in clinical practice due to a range of limitations. These shortcomings may include issues with biocompatibility, durability, or the complexity of the crosslinking process, which prevented these methods from becoming the standard process for the fabrication of clinically applied BHV.

In recent years, polyhedral oligomeric silsesquioxanes (POSS) have emerged as a promising material in the cardiovascular field of biomedical engineering [15]. The most prevalent variant is the POSS cage(hereinafter called POSS), which features a central cubic structure composed of eight silicon atoms connected to twelve oxygen atoms at the edges (Si-O-Si), with each silicon atom capable of having an organic group attached around the cage's perimeter [16]. Seifalian's group demonstrated that POSS exhibited no cytotoxicity and was capable of significantly enhancing the adhesion, proliferation, and confluence formation of endothelial cells on polymer materials via an in vitro study [17]. This finding suggests that POSS can create a more favorable cellular microenvironment on these materials, which is crucial for their potential biomedical applications. Besides, they discovered that POSS could effectively reduce the infiltration of inflammatory cells and the formation of capsules around the nanocomposite through subcutaneous implantation in sheep [18]. Moreover, another in vitro study was carried out by the group, which verified that POSS had the ability to alleviate the adhesion of fibrinogen and platelets. Additionally, POSS could decrease the formation of blood clots and increase the lysis of clots when in contact with blood. The antithrombogenic property of POSS might primarily stem from its incessant conformational changes, which endow it with unique functions in regulating blood-material interactions. [19]. Additionally, the tensile strength and elastic modulus of the nanocomposite were elevated significantly in the case of the introduction of POSS [20]. Furthermore, the anti-calcification ability of the material was strengthened by POSS, which was verified via an in vitro accelerated physiological pulsatile pressure system [21]. In summary, the incorporation of POSS cage into cardiovascular polymer materials can enhance the mechanical properties, cytocompatibility, biostability, antithrombogenicity and anti-calcification ability of these materials. Hence, POSS cage holds great potential for improving the performance and longevity of cardiovascular implants and devices [15].

Polyethylene glycol (PEG) has gained widespread application in the medical fields due to its versatile physicochemical properties [22]. The process of PEGylation, which involves coating a material's surface with PEG, can prevent enzymatic degradation, reduce immunogenic and antigenic reactions, and avoid recognition by the mononuclear phagocyte system (MPS) through a phenomenon known as the Stealth effect, which prevents proteins from adsorbing to the material surface [23,24]. It has been verified through an in vitro study that the introduction of POSS into 4-arm-PEG hydrogel is capable of enhancing the surficial roughness, as well as improving the anti-thrombosis and anti-calcification abilities of the hydrogel. Moreover, as the concentration of POSS increases within the range of 0–4 %, the aforementioned properties are further strengthened. When the decellularized heart valve was coated with POSS-PEG hybrid hydrogel, it obtained enhanced mechanical properties, improved endothelialization, heightened degradation resistance, and better anti-thrombosis and anti-calcification abilities [25,26]. A star-like eight-arm cross-linker octafunctionalized POSS of benzaldehyde-terminated polyethylene glycol (POSS-PEG-CHO) has exhibited excellent performance in the domain of diabetic wound healing [27,28]. The composite hydrogels composed of POSS-PEG-CHO and hydroxypropyltrimethyl ammonium chloride chitosan (HACC) have displayed strong mechanical strength, favorable cytocompatibility, remarkable cell proliferation, and potent antibacterial properties. Furthermore, when applied to the wounds of diabetic mice, the composite hydrogels exhibited a lower inflammatory response [28]. Actually, apart from the fact that POSS can enhance the mechanical property of materials, the larger number of cross-linking points of star polymers can also enhance their strength [29].

Although aldehydes have been criticized for their toxicity in biological crosslinking applications, their benefits are not negligible. For instance, the mechanical strength of materials can be markedly enhanced through crosslinking with aldehyde groups, and the reaction efficiency between amino groups and aldehyde groups is particularly notable. Therefore, due to the relatively low aldehyde group content in POSS-PEG-CHO than glutaraldehyde because of the high molecular weight of POSS-PEG-CHO, it is possible to create BHV with superior performance and little aldehyde content. In our study, as shown in Fig. 1, we used POSS-PEG-CHO to crosslink DPP to get POSS-PEG-PP and investigate its performance in various aspects.

2. Materials and methods

2.1. Materials

Allyl polyethylene glycol (Allyl-PEG-OH, Mn = 2 kDa) was sourced from Jiangsu Haian Petroleum Chemical Factory (Nantong, China). 1-(3-Dimethylaminopropyl)-3-ethylcarbodiimide hydrochloride (EDCI) and 2,2-Dimethoxy-2-phenylacetophenone (DMPA) were purchased from Adamas (Shanghai, China). Glutaraldehyde (50 %), citric acid, ninhydrin and ethylene glycol were obtained from Aladdin. Sodium dodecyl sulfate (SDS) was purchased from Biofroxx. Triton X-100, bovine serum albumin conjugated with fluorescein isothiocyanate (BSA-FITC), Calcein AM/PI assay kit, and Alizarin Red S solution were all acquired from Solarbio. Lucifer Yellow CH dilithium salt was sourced from MedChemExpress. Fibrinogen conjugated with fluorescein isothiocyanate (FBG-FITC) was obtained from Xi'an Ruixi Biological Technology Co., Ltd. Phosphate-buffered saline (PBS) was purchased from Biosharp. Dulbecco's Modified Eagle Medium (DMEM) and fetal bovine serum (FBS) were procured from Gibco. The LDH cytotoxicity assay kit and DAPI solution were acquired from Beyotime. Cell Counting Kit-8 (CCK-8) was obtained from Hycezmbio. CD3 antibody was sourced from Genetech, and CD68 antibody was purchased from Boster.

2.2. Synthesis of octafunctionalized POSS of benzaldehyde-terminated polyethylene glycol

POSS-PEG (2 kDa) -CHO was synthesized according to the previous reports [28]. After that, ^{1}H NMR and ^{13}C NMR were used to characterize POSS-PEG-CHO.

2.3. Preparation of DPP

In accordance with previous studies [30,31], fresh porcine pericardium (PP) was obtained from the sacrificed porcine and washed with PBS. Subsequently, the adipose tissue was gently removed from the PP. After that, the PP was then immersed in 0.5 % (v/v) solution of Triton X-100 for 12 h, followed by 0.5 % (w/w) solution of sodium dodecyl sulfate (SDS) for an additional 12 h, both at a temperature of 37 °C with continuous agitation. After this treatment, the substance was washing with deionized water three times, each time 10 min. Then, the decellularized porcine pericardium (DPP) was obtained.

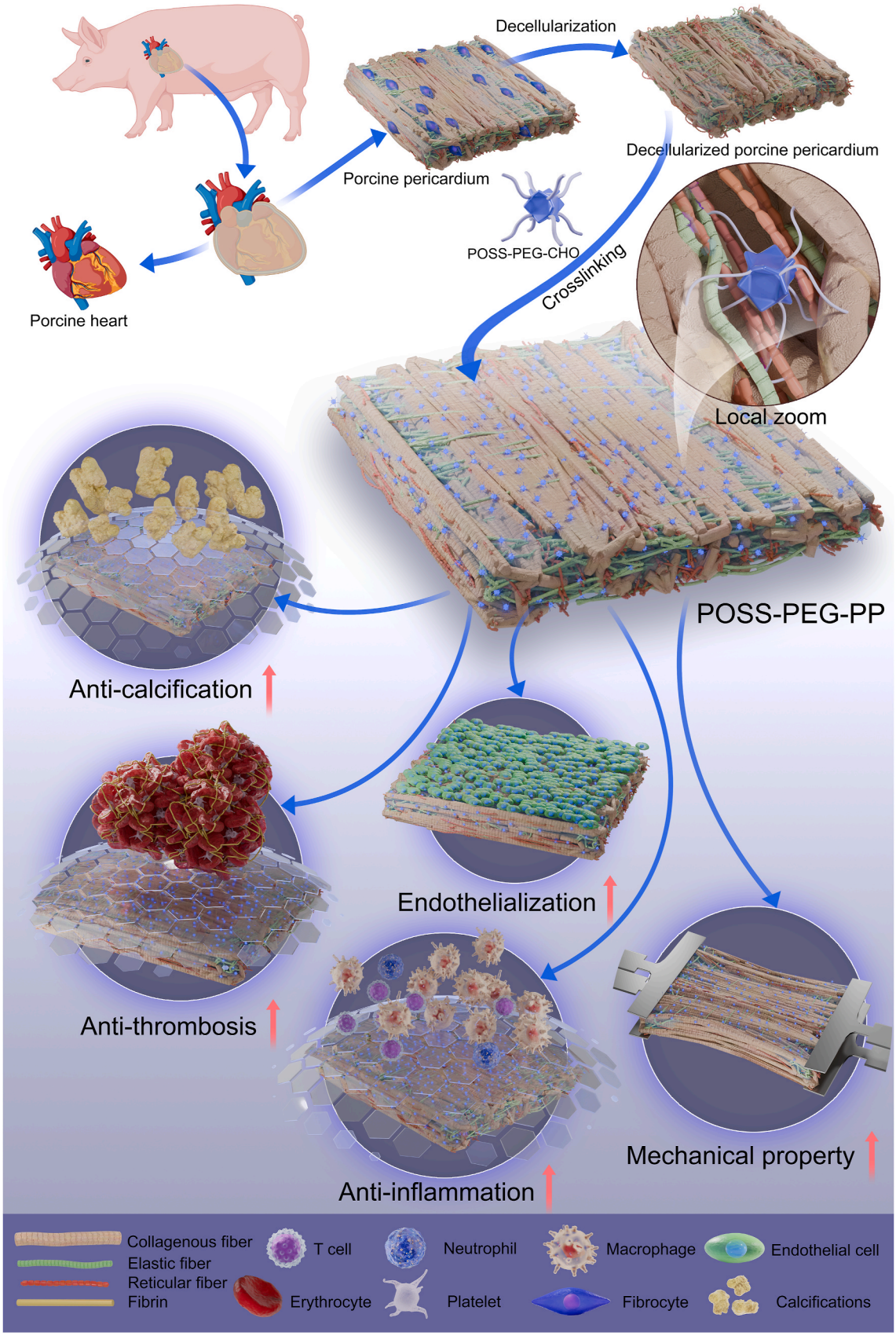

Fig. 1. The fabrication procedure of POSS-PEG-PP with pro-mechanical property, pro-endothelialization, anti-thrombosis, anti-inflammation and anti-calcification property.

2.4. Preparation of Glut-PP

DPP was soaked in 0.625 % (w/w) glutaraldehyde solution for 24 h in 37 °C with constant shaking and glutaraldehyde crosslinked porcine pericardium (GLUT-PP) was obtained. Before the tests, the Glut-PP was washed by deionized water three times with each wash lasting for 10 min.

2.5. Preparation of POSS-PEG-PP

DPP was soaked in POSS-PEG-CHO solutions at varying concentrations(10 mg/mL, 20 mg/mL, 30 mg/mL, 40 mg/mL, and 50 mg/mL) for 24 h in 37 °C with consistent shaking, respectively. Then, 5 types of POSS-PEG-CHO crosslinked porcine pericardium were obtained. Before the tests, the POSS-PEG-PP was washed with deionized water three times for 10 min each.

2.6. Amino content test

the content of materials was quantified by the ninhydrin assay. The materials were cut in to square shape (1 cm x 1 cm) and washed by deionized water for 3 times. Then, the materials were lyophilized for 24 h and weighed (W),Ninhydrin and citrate acid (0.1 M) was mixed in ethylene glycol solution to prepare the ninhydrin solution(1 mg/mL, pH = 5). The materials were immersed in 1 mL ninhydrin solution and bathed away from light at 95 °C for 1 h. After competition, the mixtures were cooled to room temperature. Then, the supernatant was transferred into a 96-well plate and absorbance at 567 nm was measured by a microplate reader. The content of amnio was calculated by the followed formulation:

$$\text{Relative Amino Content}\ (\%) = (\mathrm{OD}_{\mathrm{materials}} / W_{\mathrm{materials}}) / (\mathrm{OD}_{\mathrm{DPP}} / \mathrm{W}_{\mathrm{DPP}}) \times 100\%$$

2.7. Characterizations

DPP, GLUT-PP, and POSS-PEG-PP samples were cut into squares (10 mm x 10 mm) and sandwiched between two glass slides to maintain their shape. Subsequently, the sandwiched samples underwent a freeze-drying process. To further analyze the properties of these samples, they were then subjected to multiple advanced characterization techniques. Specifically, Attenuated total reflection Fourier-transform infrared spectroscopy (ATR-FTIR), Scanning Electron Microscope (SEM) and Atomic Force Microscope (AFM). The sample went through gold spraying in 40 mA for 60 s before SEM observation due to its non-conductive property.

2.8. Uniaxial tensile performance test

DPP, GLUT-PP and POSS-PEG-PP were cut into rectangles (30 mm x 10 mm) and the samples were soaked in PBS before test. The thickness of samples was measured and recorder by a vernier scale in three different points. Thereafter, both ends of each sample were firmly pinched into the clamps of a tensile tester. The initial lengths (L0) of samples between clamps were recorded for later analysis. The PPs were stretched within the tensile tester at a constant speed of 20 mm/min until fracture. During this process, the force–displacement curve was recorded for further analysis.

2.9. Water contact angle test

DPP, GLUT-PP and POSS-PEG-PP were cut into squares (10 mm x 10 mm) and rinsed with deionized water three times. The materials were then placed between two glass slides and freeze-dried. After drying, the samples were flattened on a smooth glass slide, and the contact angle of water was measured using a tensiometer.

2.10. Thermal shrinkage temperature test

The thermal shrinkage temperature of the samples was determined using Differential Scanning Calorimetry (DSC). DPP, GLUT-PP and POSS-PEG-PP were cut into squares (10 mm x 10 mm) and rinsed with deionized water for 3 times. Then, materials were places in between two glass slides and freeze-dried. After drying, the samples were placed in hermetically sealed pans and heated at a rate of 5 °C/min from 30 to 120 °C under nitrogen atmosphere. The maximum value of endotherm peak was recorded as thermal shrinkage temperature.

2.11. Aldehyde group content test

The aldehyde group content of the samples was quantified using the lucifer yellow CH assay. DPP, GLUT-PP, and POSS-PEG-PP samples were cut into circular patches (φ = 6 mm) and washed by deionized water for 3 times to remove any residual contaminants. Subsequently, the samples were placed in the wells of a 96-well plate and incubated with a lucifer yellow solution at a concentration of 10 μg/mL, with 500 μL per well, for 12 h. After the incubation, the samples were rinsed three times with deionized water to remove unbound lucifer yellow. The fluorescence of the bound lucifer yellow was then measured using a confocal laser scanning microscope, with an excitation wavelength set at 405 nm and an emission wavelength at 540 nm.

2.12. Protein adhesion

DPP, GLUT-PP and POSS-PEG-PP were cut into circular patches (φ = 10 mm) and washed by PBS for 3 times. Then materials were placed at the wells of a 48-well plate and incubated with either bovine serum albumin conjugated with fluorescein isothiocyanate (BSA-FITC) at a concentration of 1 mg/mL or fibrinogen conjugated with fluorescein isothiocyanate (FBG-FITC) at a concentration of 0.1 mg/mL, with 500 μL per well, at 37 °C for 2 h. Following the incubation, the samples were rinsed three times with PBS. The fluorescence of the samples was subsequently measured using a confocal laser scanning microscope, with excitation and emission wavelengths set at 488 nm and 525 nm, respectively.

2.13. In vitro cytotoxicity evaluation

L929 cells were employed to assess the in vitro cytotoxicity of the materials. DPP, GLUT-PP and POSS-PEG-PP samples were initially washed with deionized water three times to remove any contaminants. Subsequently, the samples were cut into small pieces and sterilized using 75 % ethanol for 24 h, followed by UV irradiation for 2 h. The samples were then rinsed with PBS three times to remove the residual ethanol. Complete medium was prepared with RPMI 1640 medium containing 1 % penicillin–streptomycin and 10 % fetal bovine serum. Then, the 30 cm^2 samples' pieces were rinsed in 10 mL of complete medium at 37 °C for 3 days with constant shake to obtain extract liquid. L929 cells were seeded in a 96-well plate with a density of 5×10^3 cells per well. Once the cells had adhered to the well bottom, the medium was replaced with sample extract and complete medium was set as the negative control. Cell viability was assessed using the cell counting kit-8 (CCK-8) assay at

1 day and 3 days after incubation at 37 °C in a 5 % CO_2 atmosphere. For the assay, 100 μL of Dulbecco's Modified Eagle Medium (DMEM) containing 10 % CCK-8 reagent was added to each well. After 1 h incubation, the reaction mixture was transferred to a new 96-well plate, and the absorbance at 450 nm was measured using a microplate reader. Besides, L929 cells were seeded into Confocal Dishes and cultured according to the previously described method. After 3 days culture, the cells were gently washed with PBS. Subsequently, they were incubated with the Calcein-AM/PI Assay solution at 37 °C for 30 min. Then, the L929 cells were rinsed again with PBS. Finally, the cells were examined under a confocal laser scanning microscope to evaluate their viability and morphology.

2.14. Human umbilical vein endothelial cells growth

DPP, GLUT-PP and POSS-PEG-PP were cut into circular patches (φ = 10 mm) and washed with deionized water 3 times. Then, these were sterilized with 75 % ethanol for 24 h followed by UV irradiation for 2 h. After that, the samples were rinsed in PBS 3 times to remove the residual ethanol. Sterilized samples were placed in the wells of a 48-well plate, and human umbilical vein endothelial cells (HUVECs) were seeded on the samples at a density of 1.5×10^4 cells per well. The cells were incubated at 37 °C in 5 % carbon dioxide atmosphere for 1 day, 3 days and 5 days to allow for adhesion and proliferation. The Medium was replaced per 24 h. After the accomplishment of culture, the cell viability was measured by cell counting kit-8 (CCK-8) assay. Each well was replaced by 300 μL DMEM containing 10 % CCK-8 reagent. After 1 h incubation, 100 μL reaction mixture was transferred into a new 96-well plate and absorbance at 450 nm was measured by a microplate reader. Besides, the samples cultured after 3 days and 5 days were washed with PBS, and each well was incubated with 300 μL of Calcein-AM/PI assay solution at 37 °C for 30 min. After incubation, each well was rinsed with PBS, and the samples were observed under a confocal laser scanning microscope to assess cell viability and morphology.

2.15. Hemolysis test

DPP, GLUT-PP and POSS-PEG-PP were cut into circular patches (φ = 10 mm) and washed with PBS 3 times. The samples were then placed at the wells of a 48-well plate. Fresh rat artery blood was collected with EDTA anticoagulant vacuum tube. The blood was centrifuged at 1500 r/min for 15 min to separate the components, after which the supernatant was discarded. 350 μL red blood cell suspension and 700 μL PBS were added to each well and incubated together at 37 °C for 2 h. Deionized water and PBS were set as positive control and negative control, respectively. After the completion of the incubation, the samples were removed and 1000 μL of the mixed solution was transferred into 2 mL centrifuge tubes and centrifuged at 3000 r/min for 10 min. Finally, the supernatant was transferred to a 96-well plate, and the absorbance value at 541 nm was measured using a microplate reader. The hemolysis was calculated by the followed formulation:

$$\text{Hemolysis ratio } (\%) = (OD_{material} - OD_{negative\ control} \,/\, (OD_{positive\ control} - OD_{negative\ control}) \times 100\%$$

2.16. Recalcification whole blood clotting

DPP, GLUT-PP and POSS-PEG-PP were cut into circular patches (φ = 10 mm) and washed with PBS 3 times. The samples were then placed at the wells of a 48-well plate. 500 μL fresh rat blood containing 2 % (v/v) 100 mM $CaCl_2$ were added on materials and incubated at 37 °C for 1 h to allow for thrombus formation. After incubation, the samples with thrombus were carefully transferred into new wells and washed with PBS to remove any unbound blood components before being photographed. Finally, the samples were tested by LDH cytotoxicity assay kit and the absorbance was measured at 490 nm using a microplate reader.

2.17. Platelet adhesion

DPP, GLUT-PP and POSS-PEG-PP were cut into circular patches (φ = 10 mm) and washed with PBS 3 times. Then the samples were placed at the wells of a 48-well plate. Fresh rat blood was collected and centrifuged at 1500 r/min for 15 min to separate and obtain platelet-rich plasma (PRP). Subsequently, 300 μL of PRP was added on the samples and incubated at 37 °C for 1 h to allow for platelet interaction with the samples. After incubation, the samples were tested by LDH cytotoxicity assay kit and the absorbance was measured at 490 nm using a microplate reader.

2.18. Subcutaneous implantation test

The animal experiment was approved by Ethical Committee of Zhongnan Hospital of Wuhan University. Materials were cut into squares (10 mm x 10 mm) and rinsed with deionized water three times. Then the samples were sterilized using 75 % ethanol solution for 24 h, followed by UV irradiation for 2 h. Subsequently, the samples were rinsed with PBS five times, with each rinse lasting 15 min within a biological safety cabinet to ensure a sterile environment. Subcutaneous implantation surgery was performed on Sprague Dawley rats (male, 50 ± 10 g) raised in individual ventilated cages (IVCs). Incisions were made with scalpel on the back of each rat under sodium pentobarbital (30 mg/kg) anesthesia and the samples were implanted in both sides of each incision. Each rat was implanted with 6 samples in 3 incisions. After implantation, the wounds were closed using 4-0 sutures. After 7 days, 14 days, 30 days, 60 days and 90 days of implantation, samples together with capsules were retrieved for further analysis.

2.19. Histological and immunohistochemistry analysis

Initially, samples were fixed in a 4 % paraformaldehyde solution to preserve their structure. Subsequently, the samples were dehydrated, embedded in paraffin, and sectioned into 4 mm slices. These sections were then subjected to various staining protocols to visualize different components: hematoxylin and eosin (HE) for cellular morphology, Masson's trichrome for collagen fibers, 4′, 6-diamidino-2-phenylindole (DAPI) for cell nuclei, and Alizarin Red S for calcium deposits. To specifically label immune cells, sections were treated with CD68 antibody for macrophages and CD3 antibody for T cells. The ratio of $CD3^+$ lymphocytes and $CD68^+$ macrophages was quantified by analyzing images captured at 40 x magnification.

2.20. Calcium analysis

The fibrous capsules enveloping the samples were meticulously dissected and removed, after which the samples were subjected to freeze-drying. The dried samples were then weighed and subsequently digested in 1 mL of 6 M hydrochloric acid (HCl) at a temperature of 95 °C for 12 h to solubilize the samples and release the calcium ions. Subsequently, the supernatant was carefully filtered using 40 μm filters and the filtrate was diluted with deionized water to prepare it for analysis. The calcium content of the samples was then quantified using

an inductively coupled plasma optical emission spectrometer (ICP-OES).

2.21. RNA-seq analysis

Total RNA was collected from samples including DPP, GLUT-PP, and POSS-PEG-PP after a 2 weeks subcutaneous implantation. Extraction of total RNA was performed using Trizol Reagent (Invitrogen Life Technologies). Subsequently, 3 mg RNA was applied as the input for RNA sample preparations. To generate sequencing libraries, mRNA was isolated from the total RNA using poly-T oligo-attached magnetic beads. Fragmentation was executed using divalent cations at an elevated temperature within Illumina's proprietary fragmentation buffer. First-strand cDNA was synthesized with random oligonucleotides and Super Script II. Then, second-strand cDNA synthesis was carried out using DNA Polymerase I and RNase H. Remaining overhangs were transformed into blunt ends through exonuclease/polymerase activities, and the enzymes were removed. After adenylation of the 3′ ends of the DNA fragments, Illumina PE adapter oligonucleotides were connected to prepare for hybridization. The library fragments were purified using the AMPure XP system (Beckman Coulter, Beverly, CA, USA) to select the preferred 400–500 bp cDNA fragments in length. DNA fragments with ligated adaptor molecules on both ends were selectively enriched using Illumina PCR Primer Cocktail in a 15-cycle PCR reaction. Products were purified (AMPure XP system) and quantified using the Agilent high sensitivity DNA assay on a Bioanalyzer 2100 system (Agilent). The sequencing library was then sequenced on NovaSeq 6000 platform (Illumina) Shanghai Personal Biotechnology Cp. Ltd. For bioinformatics analysis, HTSeq was used to compare the Read Count values on each gene as the original expression of the gene, and FPKM was used to standardize the expression. The difference expression of genes was analyzed by DESeq2 (v1.38.3) with screened conditions as follows: expression difference multiple $|\log2FoldChange| > 1$, significant P value < 0.05.

2.22. Statistical analysis

Data was calculated and shown as mean ± standard deviation (SD). Comparisons between two groups were analyzed with unpaired t-tests. One-way analysis of variance (ANOVA) was used for statistical analyses of multiple comparisons. $P < 0.05$ were considered statistically significant.

3. Results

3.1. Preparation of scaffolds

The synthesis of the crosslinking agent, POSS-PEG-CHO, was carried out following previously established methods. The structural integrity of POSS-PEG-CHO was confirmed through ^{1}H NMR (Fig. S1A) and ^{13}C NMR (Fig. S1B) spectroscopic analysis. As shown in Fig. 2D, HE staining, along with DAPI staining, demonstrated that cells were completely removed from the PP, resulting in DPP. Furthermore, Masson staining indicated that DPP retained the majority of the collagenous fibers from PP, with a noticeable change that the fiber arrangement became looser and more disorganized compared to the PP. POSS-PEG-PP were prepared by reacting POSS-PEG-CHO solutions of varying concentrations (10 mg/mL, 20 mg/mL, 30 mg/mL, 40 mg/mL, and 50 mg/mL) with DPP through Schiff base reaction (Fig. 2A). The crosslinking degree of POSS-PEG-PP at concentrations of 40 mg/mL and 50 mg/mL showed no significant difference and was found less than GLUT-PP (Fig. 2B). Consequently, we selected the 40 mg/mL POSS-PEG-PP for subsequent experiments. The successful fabrication of POSS-PEG-PP was validated by ATR-FTIR spectroscopy. As shown in Fig. 2C, the disappearance of the aldehyde group absorption peak at 1715 cm^{-1}, along with the emergence of characteristic peaks for Si-O-Si bonds at 1035 cm^{-1} and C-H bonds at 2882 cm^{-1}, confirmed that POSS-PEG-CHO had reacted with DPP and POSS-PEG was successfully conjugated to DPP.

3.2. Characterization

The color of POSS-PEG-PP was white in general view (Fig. S2). As shown in Fig. 2E, the surface morphology of the materials was examined using SEM. It was observed that the arrangement of the wavy fibers became more compact after the crosslinking process, with POSS-PEG-PP exhibiting a denser structure compared to GLUT-PP. Additionally, both POSS-PEG-PP and GLUT-PP maintained their integrity, showing almost no visible cracks and no fiber breakage after undergoing the freeze-drying procedure. The surface property of the materials was further tested using AFM. The two-dimensional AFM images revealed denser fiber networks for both POSS-PEG-PP and GLUT-PP. The three-dimensional AFM images provided a more detailed view of the surface topography, with POSS-PEG-PP displaying the highest roughness (Ra = 69.1 nm), followed by GLUT-PP at 67.4 nm. In contrast, DPP showed the lowest roughness, with Ra = 24.3 nm.

3.3. Physical and chemical properties

The WCA measurements for the various materials revealed distinct surface properties. The WCA of DPP was measured at 27.68 ± 0.77°. Crosslinking with GLUT resulted in an increase in WCA to 38.67 ± 2.00°, suggesting a more hydrophobic surface. Conversely, the WCA of POSS-PEG-PP decreased to 19.62 ± 0.53° (Fig. 3B), indicating a more hydrophilic surface. To evaluate the thermal stability of these materials, DSC was employed to determine the thermal shrinkage temperature. DPP demonstrated relatively poor thermal stability, with a thermal shrinkage temperature of 83.71 ± 1.47 °C. Crosslinking with GLUT or POSS-PEG-PP significantly enhanced thermal stability. The thermal shrinkage temperatures for GLUT-PP and POSS-PEG-PP were raised to 93.55 ± 2.80 °C and 89.63 ± 3.02 °C, respectively, with no significant difference observed between the two (Fig. 3G). To confirm the mechanical stability of the materials, their tensile performance was measured and analyzed. As shown in Fig. 3E, the ultimate tensile strength of DPP was 7.95 ± 1.88 MPa. The ultimate tensile strength of the other two was improved, with POSS-PEG-PP (28.90 ± 2.26 MPa) showing a significantly higher value than GLUT-PP (15.78 ± 1.30 MPa). The slope of the stress-strain curve, representing the elastic modulus, also increased for the crosslinked materials (Fig. 3A). The elastic modulus of DPP was 19.45 ± 3.23 MPa, while POSS-PEG-PP reached 97.44 ± 10.87 MPa, outperforming GLUT-PP at 28.29 ± 2.55 MPa (Fig. 3D). The content of aldehyde groups in the materials is a critical factor affecting cytocompatibility and biocompatibility. To detect residual aldehyde groups, the lucifer yellow CH assay and 2,4-dinitrophenylhydrazine assay were applied. After incubation with lucifer yellow CH solution, the color of GLUT-PP turned to green-yellow in general view, while the other two groups did not change (Fig. S3). When detected under confocal laser scanning microscope, the relative lucifer yellow fluorescence intensity in the GLUT-PP group was markedly elevated compared to the DPP group, indicating a greater abundance of residual aldehyde groups. In contrast, the POSS-PEG-PP group exhibited low fluorescence intensity that was not significantly different from the DPP group (Fig. 3C and F). The 2,4-dinitrophenylhydrazine experiment results (Fig. S7A and B) corroborated lucifer yellow CH assay results, indicating low level of residual aldehyde groups of POSS-PEG-PP, which is advantageous for cytocompatibility and biocompatibility.

3.4. Cytocompatibility

To evaluate the cytotoxicity of the materials, L929 cells were exposed to extracts derived from the different materials. Cell viability was evaluated using the CCK8 assay at two time points: 1 day and 3 days post-exposure. Additionally, the cellular survival status was assessed on day 3 using the Calcein AM/PI Assay. The CCK8 assay results demonstrated that both DPP and POSS-PEG-PP did not exhibit significant difference in cell viability when compared to the negative control

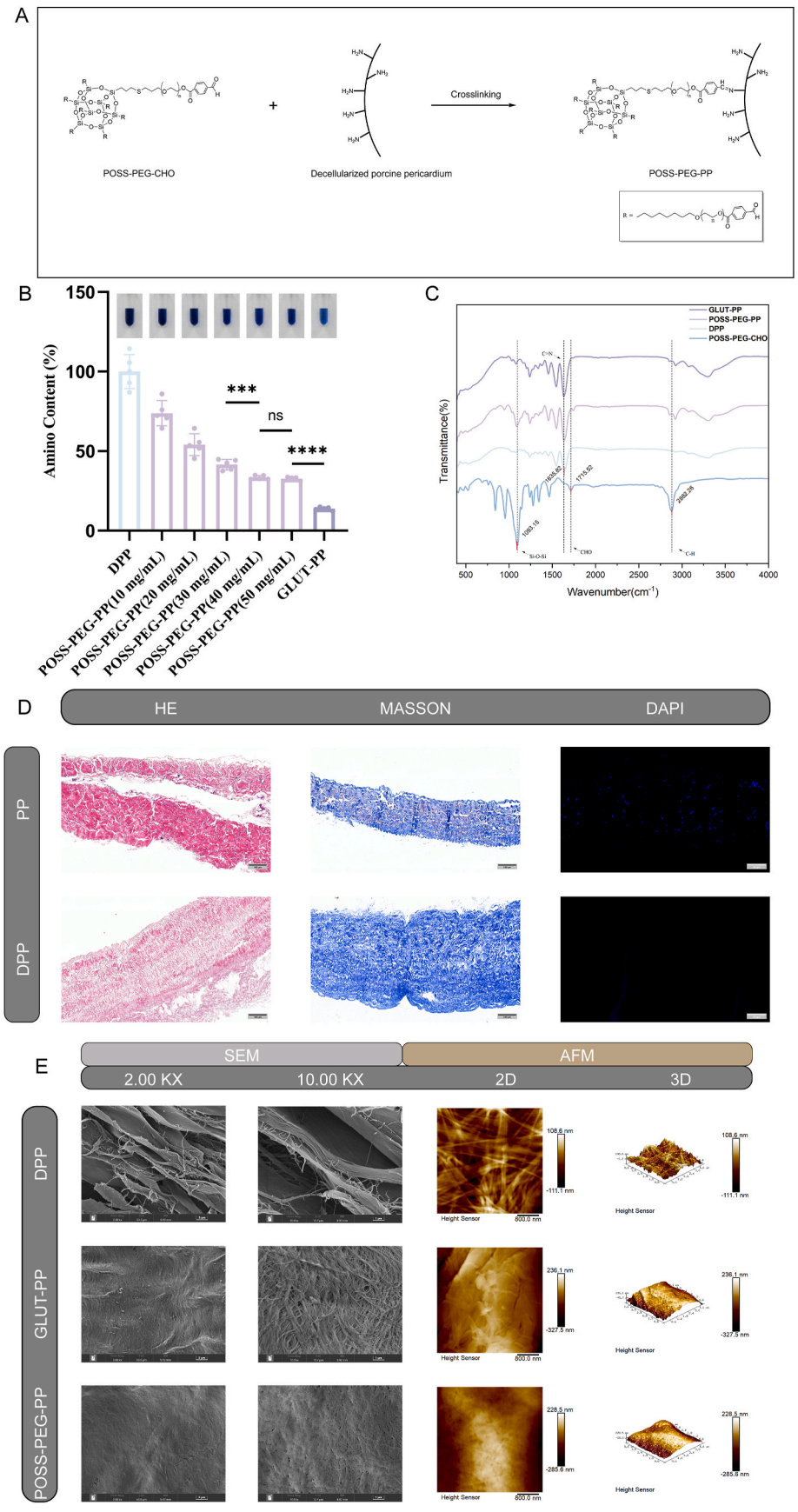

(caption on next page)

Fig. 2. Preparation and characterization of materials. (A) Scheme of the reaction between POSS-PEG-CHO and DPP. (B) Amino content of DPP, GLUT-PP and POSS-PEG-PP (10 mg/mL, 20 mg/mL, 30 mg/mL, 40 mg/mL and 50 mg/mL). (C) The FTIR spectra of POSS-PEG-CHO, DPP, POSS-PEG-PP and GLUT-PP. (D) HE, Masson and DAPI staining of PP and DPP. (E) SEM and AFM images of the surface morphology of DPP, GLUT-PP and POSS-PEG-PP. Data are expressed as the mean ± SD, $*p < 0.05$, $**p < 0.01$, $***p < 0.001$, and $****p < 0.0001$.

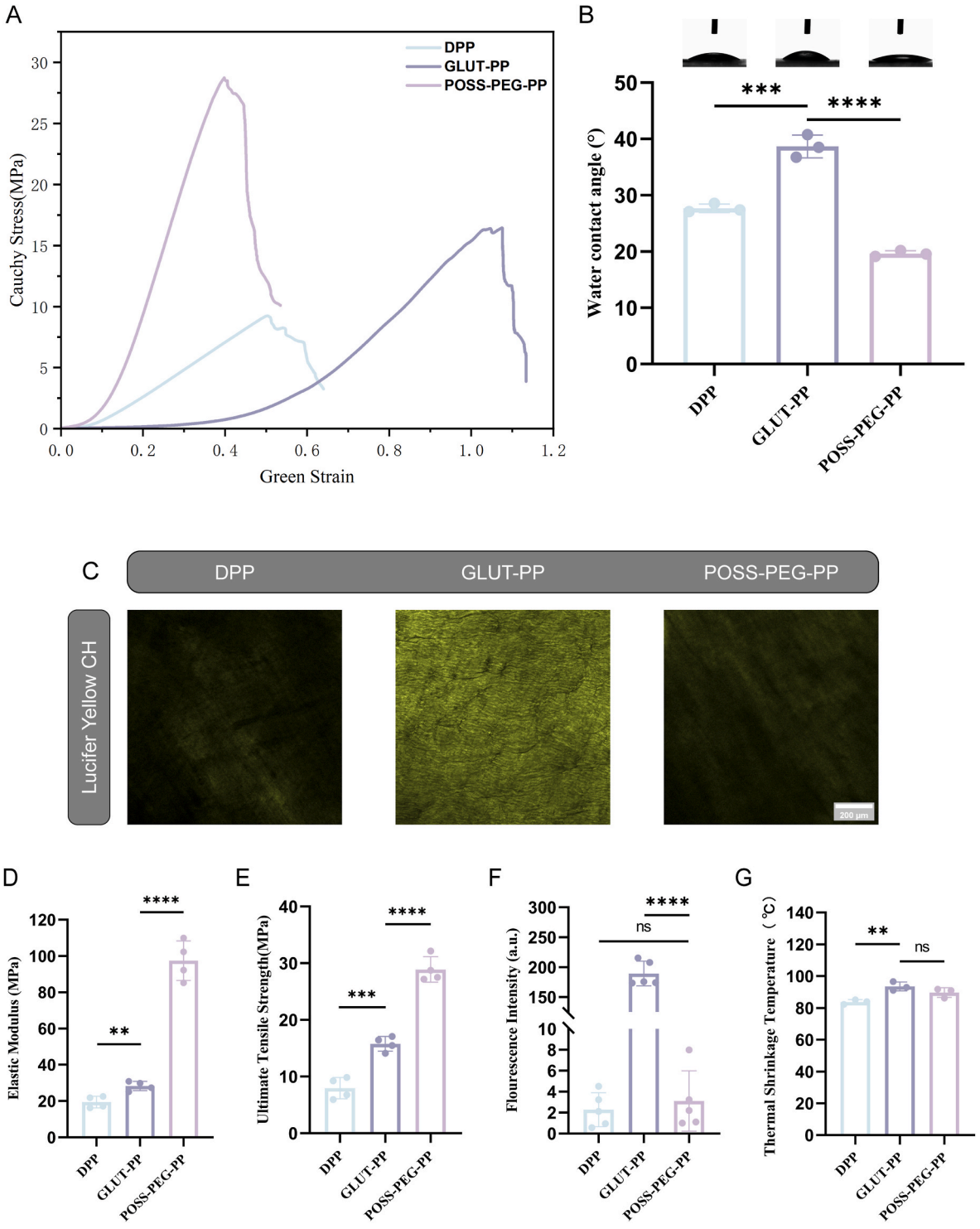

Fig. 3. Physical and chemical properties of materials. (A) The strain–stress curve of DPP, GLUT-PP and POSS-PEG-PP. (B) The water contact angle of DPP, GLUT-PP and POSS-PEG-PP. (C) Lucifer yellow CH staining images of DPP, GLUT-PP and POSS-PEG-PP. (D) The Elastic modulus of DPP, GLUT-PP and POSS-PEG-PP. (E) The ultimate tensile strength of DPP, GLUT-PP and POSS-PEG-PP. (F) Fluorescence intensity of DPP, GLUT-PP and POSS-PEG-PP after lucifer yellow CH staining. (G) The thermal shrinkage temperature of DPP, GLUT-PP and POSS-PEG-PP. Data are expressed as the mean ± SD, $*p < 0.05$, $**p < 0.01$, $***p < 0.001$, and $****p < 0.0001$. (For interpretation of the references to color in this figure legend, the reader is referred to the Web version of this article.)

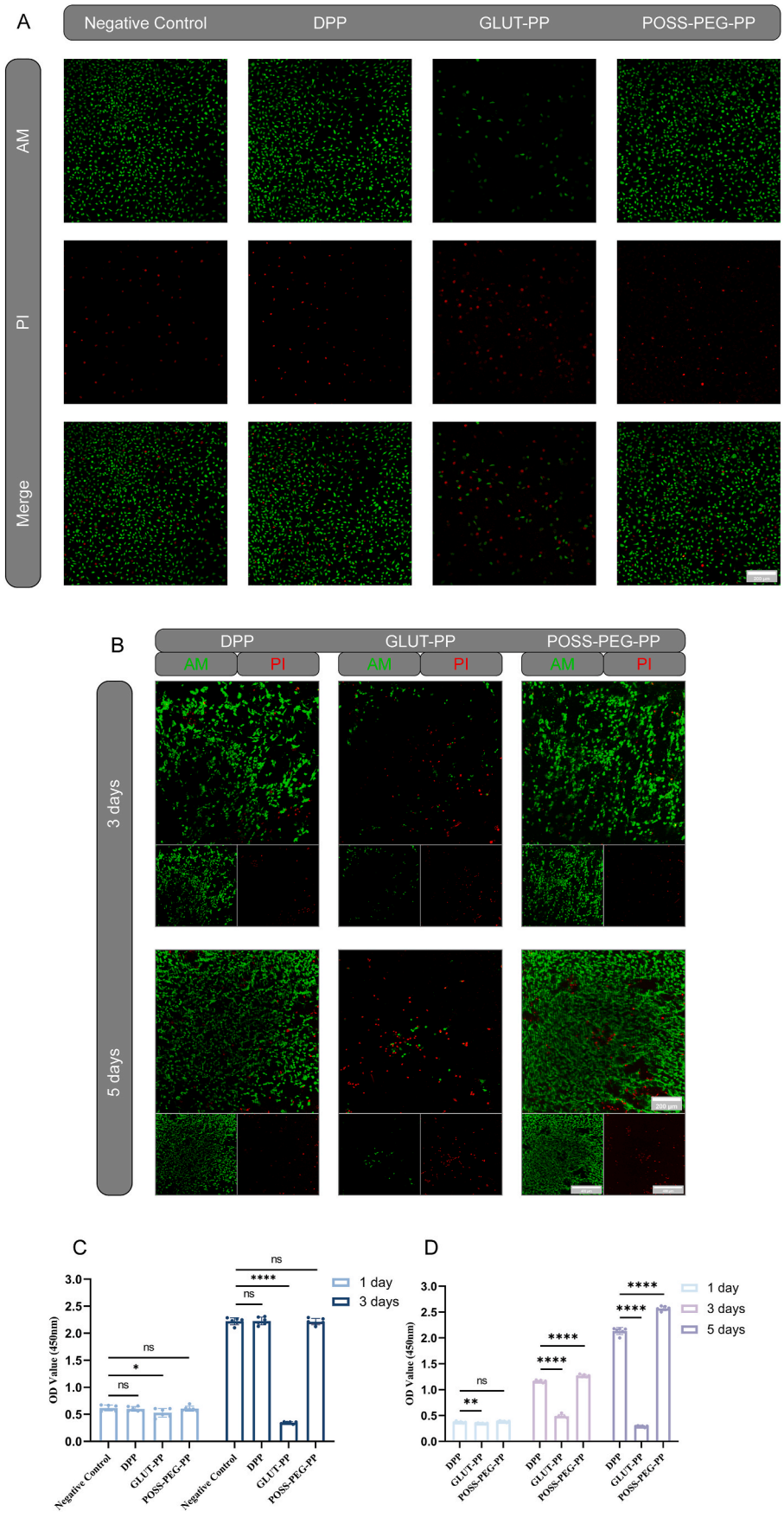

(caption on next page)

Fig. 4. Cytocompatibility of materials. (A) Calcein-AM/PI staining images of L929 cells cultured for 3 days in the extracts of DPP, GLUT-PP and POSS-PEG-PP. (B) Calcein-AM/PI staining images of HUVECs grown on the surface of DPP, GLUT-PP and POSS-PEG-PP. (C) CCK8 assay quantification of the viability of L929 cells cultured in the extract of DPP, GLUT-PP and POSS-PEG-PP. (D) CCK8 assay quantification of the viability of HUVECs grown on the surface of DPP, GLUT-PP and POSS-PEG-PP. Data are expressed as the mean ± SD, $*p < 0.05$, $**p < 0.01$, $***p < 0.001$, and $****p < 0.0001$.

(complete medium) after both 1 day and 3 days of culture. In contrast, the GLUT-PP group displayed significant cytotoxicity relative to the negative control, with a particularly obvious effect observed on day 3 (Fig. 4C). This suggests that GLUT-PP has a higher cytotoxic potential compared to DPP and POSS-PEG-PP, while there was no significant difference in cytotoxicity between DPP and POSS-PEG-PP. The Calcein AM/PI staining images (Fig. 4A) corroborated the findings from the CCK8 assay, further validating the observed trends in the cytotoxicity of materials. To assess the adhesion and proliferation of HUVECs on various materials, HUVECs were cultured on these substrates, and their viability was evaluated using the CCK8 assay at 1 day, 3 days and 5 days post-seeding. Additionally, the Calcein AM/PI assay was employed for visual confirmation of cell viability at 3 days and 5 days post-seeding. The CCK8 assay results indicated that both the POSS-PEG-PP and DPP groups fostered superior adhesion and proliferation of HUVECs compared to the GLUT-PP group, with the POSS-PEG-PP group demonstrating the most robust function (Fig. 4D). The cell survival staining images (Fig. 4B and Fig. S4) confirmed the CCK8 results, showing a higher density of live cells on POSS-PEG-PP and DPP compared to GLUT-PP. Furthermore, the images revealed the formation of endothelial cell confluence on POSS-PEG-PP by day 5. This observation is significant as it indicates that POSS-PEG-PP not only supports HUVECs adhesion and proliferation but also facilitates the development of a confluent monolayer, which is a crucial step in the formation of a functional endothelium.

3.5. Hemocompatibility

Thrombosis is a complex process that initiated by the non-specific adsorption of proteins. To assess the protein adsorption properties of the materials, BSA and FBG adhesion assays were conducted. The findings demonstrated that POSS-PEG-PP significantly resisted protein adsorption compared to the other materials (Fig. 5A, B and C). Regarding platelet adhesion, LDH assays and SEM were utilized to evaluate the performance. The results indicated a substantial number of platelets adhered to the surfaces of DPP and GLUT-PP, whereas only a few attached to POSS-PEG-PP (Fig. 5H and I). This suggests that POSS-PEG-PP possesses a propensity to repel platelet adhesion. For a more comprehensive verification, recalcification whole blood clotting assay was performed. As depicted in Fig. 5F and G, numerous blood clots were observed on the surfaces of DPP and GLUT-PP, whereas only a few clots adhered to POSS-PEG-PP. This observation implies that POSS-PEG-PP exhibits a superior anti-thrombotic property. Hemolysis, an indicator of erythrocyte compatibility, was also assessed as part of the evaluation of material safety for blood contact. The hemolytic ratios for DPP, GLUT-PP, and POSS-PEG-PP all were within the safety standards for materials in contact with blood (hemolysis rate <2 %) according to ISO 10993-1 (Fig. 5D and E).

3.6. In vivo inflammation evaluation

The immunogenicity of biomaterials is a critical factor in the degeneration of BHV, with T lymphocytes and macrophages playing an essential role in immune responses. To assess in vivo immunogenicity of the materials, subcutaneous implantation of materials in rats was conducted, with samples retrieved after 1 week and 2 weeks for further analysis. The presence of T lymphocytes and macrophages was identified through positive staining for CD3 and CD68, respectively. HE staining revealed that the inflammatory cell infiltration around POSS-PEG-PP was less compared to the other two groups. Immunohistochemical staining results indicated that POSS-PEG-PP recruited the fewest CD3-positive T cells (Fig. 6A and B) and CD68-positive macrophages (Fig. 6A and C) among the three groups, suggesting lower immunogenicity. These findings imply that POSS-PEG-PP has a capacity to escape from immune system, which is a desirable attribute for biomaterials intended for long-term implantation in body.

3.7. In vivo calcification and degradation evaluation

Calcification is a major factor affecting the longevity of bioprosthetic heart valves, and the ability to resist calcification is an essential evaluation criterion for new materials intended for use in prosthetic valves. Similar to in vivo inflammation evaluation, in vivo calcification assessment also used rat subcutaneous implantation model and the implants were retrieved after 1 month, 2 months and 3 months for further analysis. HE was utilized to evaluate the whole performance. Alizarin red staining and ICP-OES were employed to detect calcium salt content, while Masson staining was used to assess the degradation of collagen fibers. As shown in Fig. 7A, the results showed that POSS-PEG-PP displayed a good biocompatibility with the angiogenesis in the material. It also demonstrated that POSS-PEG-PP exhibited superior anti-calcification capabilities (Fig. 7B) and the majority of collagen fibers remained intact after three months of subcutaneous implantation, in contrast to GLUT-PP. This finding is significant as it suggests that POSS-PEG-PP not only effectively resists calcification but also maintains the structural integrity of collagen fibers, which is vital for the durability and functionality of bioprosthetic heart valves.

3.8. RNA-seq analysis

To investigate the mechanism of POSS-PEG-PP in the regulation of inflammation and calcification, we performed RNA-seq analysis of 2 weeks subcutaneous implants of DPP, GLUT-PP and POSS-PEG-PP. Gene heatmaps and the top 20 differentially expressed genes (DEGs) are shown in Fig. 8A. Moreover, the trend of 9 gene clusters is shown in Fig. 8B and the difference among the 3 groups is obvious. The statistics on the results of Differentially expressed genes (DEGs) of three comparison groups (DPP vs GLUT-PP, DPP vs POSS-PEG-PP and GLUT-PP vs POSS-PEG-PP) were shown in Fig. S5A. There are 40 DEGs appearing in all three comparison groups (Fig. 8C). DEGs between DPP and POSS-PEG-PP were identified via the volcano plot (Fig. 8D), which showed that 196 genes were up-regulated and 320 genes were down-regulated in POSS-PEG-PP groups [log2(fold change) > 1, P < 0.05]. The volcano plots of the other two comparison groups were shown in Figs. S5B and C. Gene Ontology Enrichment analysis suggested significant associations of the DEGs with immune system process, immune response, cell differentiation, complement activation and signaling receptor binding (Fig. 8E). The KEGG (Kyoto Encyclopedia of Genes and Genomes) enrichment analysis showed the different performance between DPP and POSS-PEG-PP is related to AMP-activated protein kinase (AMPK) and IL-17 signaling pathways (Fig. 8F). Gene ontology and KEGG enrichment of comparison between DPP and GLUT-PP was shown in Figs. S5D and E, and the osteoclast differentiation pathway was significantly changed. GO Gene Set Enrichment Analysis of the group (DPP vs POSS-PEG-PP) suggested that the biological performance of POSS-PEG-PP was significantly related to cell differentiation (Fig. S6A), negative regulation of immune system process (Fig. S6B), negative regulation of leukocyte activation (Fig. S6C), negative regulation of lymphocyte activation (Fig. S6D). Besides, KEGG Gene Set Enrichment Analysis of the group (DPP vs POSS-PEG-PP) was shown in Fig. S6E and it indicated the AMPK

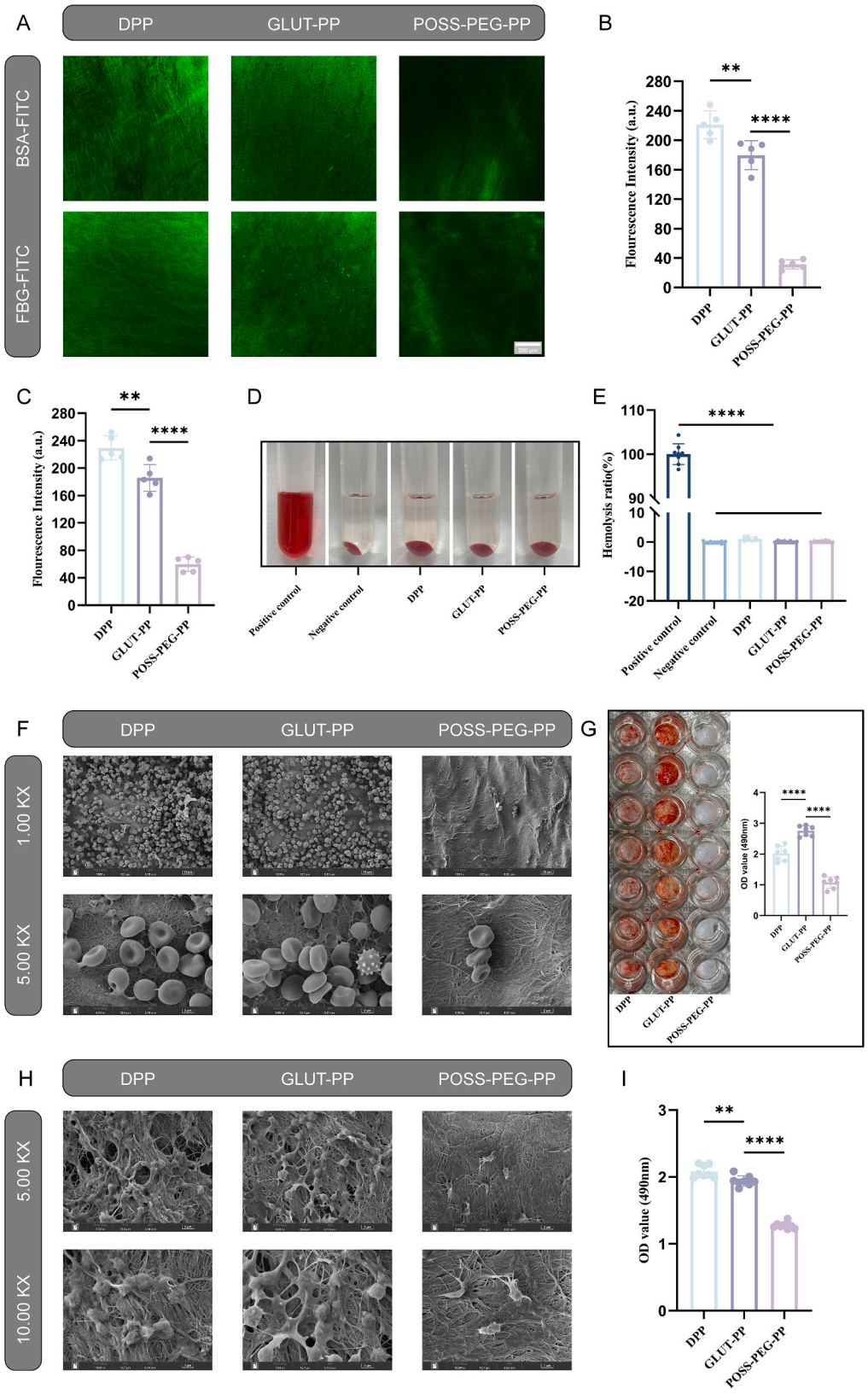

Fig. 5. Hemocompatibility of materials. (A) Confocal fluorescence microscope images of adhered BSA-FITC and FBG-FITC on the surface of DPP, GLUT-PP and POSS-PEG-PP. (B) Fluorescence intensity of DPP, GLUT-PP and POSS-PEG-PP after 2 h incubation with BSA-FITC. (C) Fluorescence intensity of DPP, GLUT-PP and POSS-PEG-PP after 2 h incubation with FBG-FITC. (D) The representative images of hemolysis. (E) The quantification of the supernatant at OD 490 nm of DPP, GLUT-PP and POSS-PEG-PP. (F) SEM images of the clot on the surface on DPP, GLUT-PP and POSS-PEG-PP. (G) The representative images of clot and the relative content of blood cells quantified by LDH assay on the surface of DPP, GLUT-PP and POSS-PEG-PP. (H) SEM images of the platelets adhered on the surface of DPP, GLUT-PP and POSS-PEG-PP. (I) The relative content quantification of the platelets adhered on the surface of DPP, GLUT-PP and POSS-PEG-PP by LDH assay. Data are expressed as the mean ± SD, $*p < 0.05$, $**p < 0.01$, $***p < 0.001$, and $****p < 0.0001$.

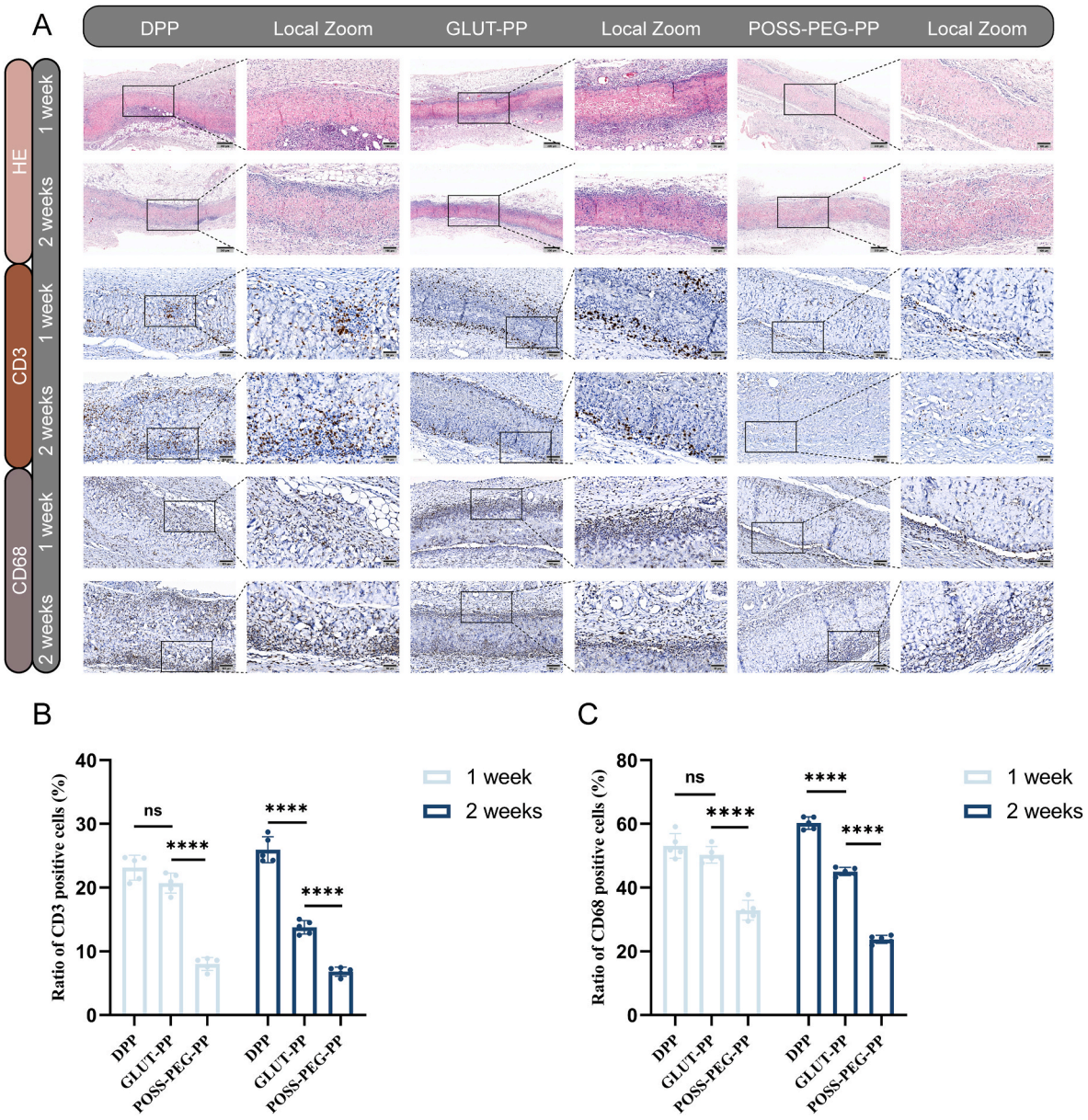

Fig. 6. In vivo inflammation evaluation of materials. (A) HE staining, CD3 immunohistochemical staining and CD68 immunohistochemical staining images of DPP, GLUT-PP and POSS-PEG-PP after 1 week and 2 weeks implantation. (B) The ratio of CD3-positive cells around DPP, GLUT-PP and POSS-PEG-PP after 1 week and 2 weeks implantation. (C) The ratio of CD68-positive cells around DPP, GLUT-PP and POSS-PEG-PP after 1 week and 2 weeks subcutaneous implantation. Data are expressed as the mean ± SD, $^{*}p < 0.05$, $^{**}p < 0.01$, $^{***}p < 0.001$, and $^{****}p < 0.0001$.

signal pathway of POSS-PEG-PP was down-regulated.

4. Discussion

The decellularization of porcine pericardium is essential for the fabrication of BHV due to its inherent immunogenicity. However, this procedure often results in a more loosely arranged fiber structure and a corresponding reduction in mechanical properties [32]. Due to the complex hemodynamic environment and the billions of cycles of opening and closing that heart valves must endure, it is vital to enhance the mechanical property of DPP. Traditionally, most commercially available biological heart valves have utilized glutaraldehyde crosslinking to bolster the mechanical strength of DPP. Nonetheless, GLUT-PP behaves poorly in cytocompatibility, hemocompatibility, and anti-calcification properties [33]. In light of these limitations, we have opted to utilize POSS-PEG-CHO as crosslinking agent for DPP. Firstly, POSS-PEG-CHO reacted with decellularized porcine pericardium (DPP) based on the Schiff's base reaction between the amino group within DPP and the aldehyde group within POSS-PEG-CHO. And the fiber arrangement changed after reaction mainly because of the star-like eight-arm branches structure of POSS-PEG and the rigidity of POSS. Therefore, the surface topography and the structural stability were altered. Besides, the properties of material were improved with the introduction of POSS and PEG. Such as, hydrophilicity, anti-thrombotic ability, immune regulation ability, anti-calcific ability and so on. At a deeper level, the mechanism of biological performances of POSS-PEG-PP involved cell differentiation, negative regulation of immune system process, negative regulation of leukocyte activation, negative regulation of lymphocyte activation and down-regulation of AMPK signaling pathway.

The arrangement of fibers of POSS-PEG-PP is notably more compact compared to GLUT-PP, which aligns with our mechanical testing outcomes. These results indicate that POSS-PEG-PP possesses superior

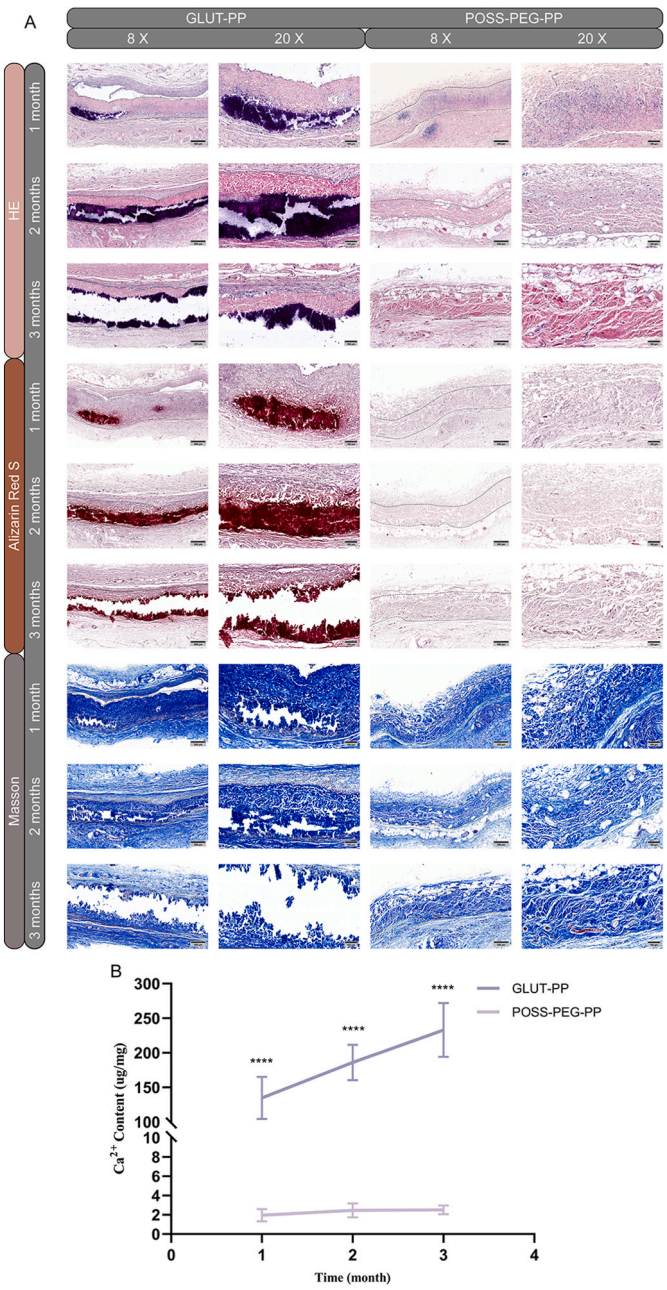

Fig. 7. In vivo calcification and degradation evaluation of materials. (A) HE, Alizarin Red S and Masson staining of GLUT-PP and POSS-PEG-PP after 1 month and 2 months and 3 months implantation. (B) Quantitative analysis of calcium content of DPP, GLUT-PP and POSS-PEG-PP after subcutaneous implantation for 1 month, 2 months and 3 months measured by ICP-OES. Data are expressed as the mean ± SD, $*p < 0.05$, $**p < 0.01$, $***p < 0.001$, and $****p < 0.0001$. (For interpretation of the references to color in this figure legend, the reader is referred to the Web version of this article.)

ultimate tensile strength and tangent modulus, endowing it with enhanced resilience against the pressures of bloodstream. The superior mechanical performance of POSS-PEG-PP is mainly attributable to the star-like eight-arm branches structure of POSS-PEG and the rigidity of POSS having a strong framework with shorter bond lengths [20]. Additionally, POSS-PEG-PP exhibits good thermal stability, indicating an excellent structural stability [34]. Hydrophilicity refers to the physical property of a substance that exhibits a strong affinity for water, allowing it to interact, dissolve, or become wetted by water. POSS-PEG-PP showed a more hydrophilic surface than both DPP and GLUT-PP mainly because of a multitude of C-O-C of PEG exiting on the surface of POSS-PEG-PP. The hydrophilicity of materials' surface is closely related to the anti-thrombotic ability. Hydrophilic surfaces have less blood protein adsorption which is the initiating event of thrombosis than hydrophobic surfaces [35]. And less platelets adhere to the hydrophilic surfaces than hydrophobic surfaces because less fibrinogen which is necessary for platelet adhesion is retained on the hydrophilic surfaces [35–37]. Therefore, the hydrophilicity of POSS-PEG-PP makes a significant contribution to the antithrombotic performance. Roughness refers to the microscopic irregularities or deviations on a surface of a material. The direct relationship between the material's roughness and the material hemocompatibility is controversial. However, it has been demonstrated that the rough surface topography could facilitate the adhesion, proliferation and migration of HUVECs [38,39]. And the formation endothelial surface layer could endow material with anti-thrombotic and immune regulation ability [40,41]. Hence, the rough surface topography of POSS-PEG-PP could foster endothelialization process and further regulate anti-thrombotic and anti-inflammatory property.

Cytocompatibility especially non-cytotoxicity and endothelialization are crucial for BHV. The toxicity of implanted materials, such as GLUT-PP, can lead to the death of surrounding cell and the local inflammation. The toxicity of GLUT-PP is mainly attributed to the residual aldehyde groups [42]. In contrast, POSS-PEG-PP has been shown to have fewer residual aldehyde groups compared to GLUT-PP because of the relative scarcity of aldehyde groups available for reaction with amines due to the high molecular weight of POSS-PEG-CHO and the insufficient cross-linking degree. Therefore, the L929 cell proliferation test showed POSS-PEG-PP was nontoxic. The endothelialization of BHV plays a pivotal role as a natural defense function, effectively preventing the accumulation of calcium ions and resisting the adhesion of fibrin and platelets. Hence, it is critically important in the prevention of thrombosis, a significant complication associated with cardiovascular implants. Therefore, enhancing the adhesion and proliferation of endothelial cells on the surfaces of cardiovascular materials is vital for reducing post-implantation complications. In our study, POSS-PEG-PP demonstrated superior performance in endothelialization. The rough surface of POSS-PEG-PP could contribute to the enhanced endothelialization observed in POSS-PEG-PP [43,44]. This characteristic is particularly important as it could lead to improved biocompatibility, reduced thrombogenicity and calcification, thereby potentially extending the lifespan and functionality of the bioprosthetic heart valves [45].

Hemocompatibility is a critical evaluative indicator for BHV due to their direct contact with blood [46]. Erythrocyte safety is of primary importance, as reflected by the hemolysis test. In the study, POSS-PEG-PP has demonstrated no potential for erythrocyte toxicity, indicating its safety in terms of erythrocyte interaction. Additionally, the ability to resist thrombosis is essential for blood-contacting medical devices because the detached thrombus can be carried by the bloodstream and blocks blood vessels in the body. Besides, the attached thrombus can lead to dysfunction and degeneration of BHV [47,48]. The formation of thrombosis is a complex process involving the activation, adhesion, and interaction of various serum proteins and blood cells. The adhesion of serum albumin, especially fibrinogen, is associated with the risk of thrombosis. Moreover, arterial thrombosis is primarily induced by the activation and adhesion of platelets. The incorporation of POSS could alleviate the binding strength fibrinogen to material and further decrease the adhesion of platelets which needs a stable configuration of fibrinogen formation due to the POSS-induced surface reorientation. Therefore, POSS could affect the process of thrombosis and thrombolysis when in contact with blood. Besides, POSS could inhibit Factors Xa activity which is vital for the formation of clots [19]. Furthermore, the high surface hydrophilicity of PEG contributes to the resistance against the adsorption of plasma proteins and platelet adhesion. These properties collectively result in POSS-PEG-PP exhibiting superior anti-thrombotic capabilities compared to GLUT-PP and DPP. In

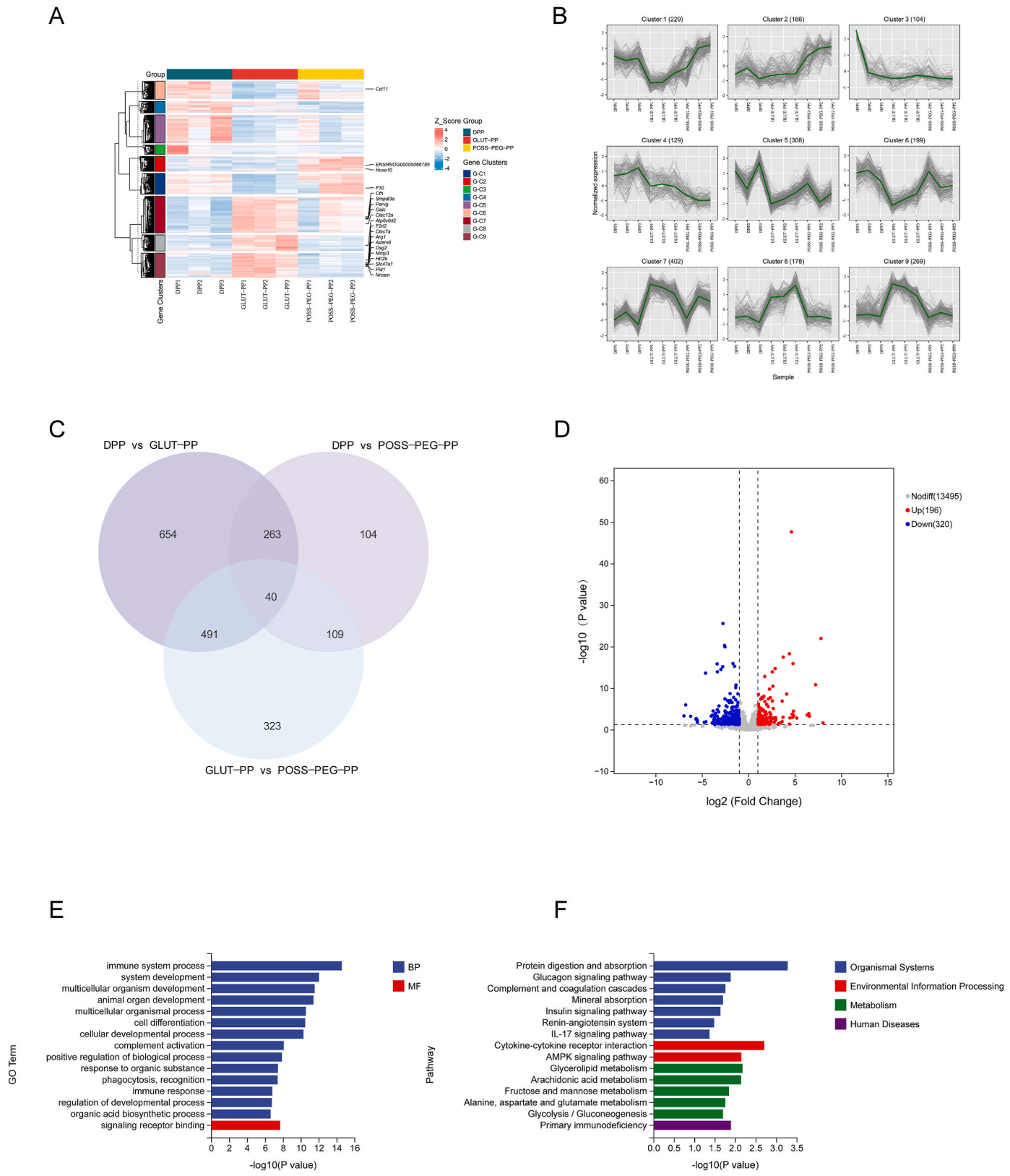

Fig. 8. RNA sequencing analysis of materials after 2 weeks implantation. (A) Gene heatmap and the top 20 differentially expressed genes of DPP, GLUT-PP and POSS-PEG-PP after 2 weeks implantation. (B) The trend of 9 gene clusters. (C) DEGs Venn diagram of the 3 comparison groups (DPP vs GLUT-PP, DPP vs POSS-PEG-PP and GLUT-PP vs POSS-PEG-PP). (D) the volcano plot of DEGs (DPP vs POSS-PEG-PP, DPP as the control). (E) Gene Ontology Enrichment analysis of DEGs of DPP vs POSS-PEG-PP. (F) KEGG enrichment analysis of DEGs of DPP vs POSS-PEG-PP.

summary, the combination of POSS and PEG in POSS-PEG-PP endows the material with enhanced hemocompatibility, reducing the risk of thrombosis and making it a promising candidate for use in biological heart valves.

The deterioration of biological heart valves is significantly associated with immune reactions, especially in the case of xenogenic tissue heart valves [49]. Reducing the immunogenicity of BHV could decrease the deposition of calcific foci, which is a key factor influencing the longevity of the valve [6,50]. Macrophages and T lymphocytes play a significant role in the immune response process. Specifically, macrophages serve as a crucial link between innate and adaptive immunity by processing antigens and presenting them to the HLA system [51]. Meanwhile, T lymphocytes are essential for adaptive immune responses and the maintenance of immune homeostasis [52]. The infiltration of macrophages and T lymphocytes is less in POSS-PEG-PP, mainly due to the "Stealth" effect of PEG and the low inflammatory response property of POSS. To further investigate the mechanism of POSS-PEG-PP in the regulation of inflammation, RNA-seq analysis was performed on 2 weeks subcutaneous implants of DPP, GLUT-PP, and POSS-PEG-PP. GO enrichment analysis suggested significant associations of the DEGs with multiple aspects, including immune system processes, immune responses, cell differentiation, complement activation, and signaling receptor binding. And our further analysis indicates that the biological performance of POSS-PEG-PP is significantly associated with negative regulation of immune system process, negative regulation of leukocyte activation, negative regulation of lymphocyte activation. Moreover, KEGG enrichment analysis revealed that the performance difference between DPP and POSS-PEG-PP is related to the intervention of the AMPK and IL-17 signaling pathways. The AMPK signaling pathway participates in numerous biological processes by regulating cellular energy homeostasis under conditions such as glucose deprivation, hypoxia, and ischemia. On one hand, the activation of the AMPK signaling pathway can elevate the energy metabolic level and reduce the content of reactive oxygen species (ROS), thereby decreasing inflammatory factors. On the other hand, blockade of the AMPK signaling pathway can influence the activity of immune cells and decrease the immune response to exogenous implants [53,54]. The IL-17 signaling pathway is crucial in innate immunity and the inflammatory response, particularly in the recruitment and activation of neutrophils [55,56]. Therefore, the intervention of AMPK and IL-17 signaling pathways play an important role in the anti-inflammatory performance of POSS-PEG-PP. As for AMPK signaling pathway, we inferred that the down-regulation of it played the primary role in the anti-inflammation process. Two main reasons are following. Firstly, the results indicated that the dominant cell infiltrating and surrounding materials was immune cell (especially macrophage) in the first two weeks. Besides, KEGG Gene Set Enrichment Analysis of the group (DPP vs POSS-PEG-PP) indicated the AMPK signal pathway of POSS-PEG-PP was in down-regulation.

Structural valve degeneration (SVD) is indeed a prevalent, inevitable, and currently untreatable outcome following BHV implantation [57]. It is characterized by an irreversible process that includes several pathological progressions such as pannus growth, leaflet fibrosis, calcification, delamination of connective tissue, and the emergence of ruptures and perforations [58]. Calcification, the most common manifestation of SVD, can cause the BHV to harden, thereby affecting its opening and closing movements [59]. The calcific pathogenesis of BHV is complex and primarily caused by inflammatory reactions, immune responses and subclinical leaflet thrombosis [60]. Additionally, The RNA-seq analysis indicated that the calcification of BHV may have something to do with osteoclast differentiation. In our study, POSS-PEG-PP demonstrated excellent anti-calcification properties, which could be partly attributed to its superior endothelialization and biocompatibility. Notably, the reduced inflammatory responses and diminished immunogenicity play a crucial role in its ability to resist calcification, suggesting that POSS-PEG-PP is expected to have an extended lifespan.

5. Conclusion

In this study, we crosslinked DPP with eight-arm cross-linker octa-functionalized POSS of PEG to obtain POSS-PEG-PP based on the Schiff's base reaction between the amino group within DPP and the aldehyde group within POSS-PEG-CHO. And it showed eminent performance in the mechanical property, endothelialization, hemocompatibility, biocompatibility, anti-inflammation and anti-calcification ability in comparison to the traditional glutaraldehyde crosslinked BHV. Then, we carried out RNA seq analysis for further mechanism investigation and we found that the intervention of AMPK and IL-17 signaling pathways may play an important role in the anti-inflammatory performance of POSS-PEG-PP and it is worth conducting in-depth research. Further large animal experiments are needed for the novel material, and POSS-PEG-PP is expected for clinical transformation.

CRediT authorship contribution statement

Xiaobo Yu: Writing – review & editing, Writing – original draft, Visualization, Validation, Project administration, Methodology, Investigation, Formal analysis, Data curation, Conceptualization. **Jingli Ding:** Writing – review & editing, Supervision, Resources, Project administration, Methodology, Funding acquisition, Formal analysis, Data curation. **Yingjie He:** Writing – review & editing, Visualization, Validation, Project administration, Methodology, Formal analysis, Data curation. **Shunbo Wei:** Methodology, Formal analysis, Data curation. **Xing Chen:** Project administration, Methodology, Formal analysis. **Qiujie Luo:** Methodology. **Yuqing Zhang:** Validation. **Chen Qian:** Methodology, Formal analysis. **Jiahui Wang:** Methodology. **Mengjie Hu:** Methodology. **Xiang Zhang:** Visualization. **Cuifen Lu:** Writing – review & editing, Supervision, Resources, Project administration, Methodology, Investigation, Formal analysis, Conceptualization. **Jinping Liu:** Writing – review & editing, Resources, Project administration, Funding acquisition, Conceptualization. **Jianliang Zhou:** Writing – review & editing, Resources, Project administration, Methodology, Funding acquisition, Formal analysis, Data curation, Conceptualization.

Funding

This work was supported by the National Natural Science Foundation of China (grant numbers 82270382, 82170505), the Natural Science Foundation of Jiangxi Province (grant numbers 20212ACB206020), the Natural Science Foundation of Hubei Province (2023AFB817), Key Research and Development Project of Hubei Provincial Department of Science and Technology (2023BCB002), Wuhan Talent's Industry-Leading Talent Project (WHYCCYLJ2021002), the talent Project of Zhongnan Hospital of Wuhan University (grant no. rcyj20210601 and CXPY2022046).

Declaration of competing interest

The authors declare that they have no known competing financial interests or personal relationships that could have appeared to influence the work reported in this paper.

Appendix A. Supplementary data

Supplementary data to this article can be found online at https://doi.org/10.1016/j.mtbio.2025.101677.

Data availability

Data will be made available on request.

References

[1] Global fertility in 204 countries and territories, 1950-2021, with forecasts to 2100: a comprehensive demographic analysis for the Global Burden of Disease Study 2021, Lancet 403 (10440) (2024) 2057–2099.

[2] S. Coffey, R. Roberts-Thomson, A. Brown, J. Carapetis, M. Chen, M. Enriquez-Sarano, L. Zühlke, B.D. Prendergast, Global epidemiology of valvular heart disease, Nat. Rev. Cardiol. 18 (12) (2021) 853–864.

[3] T. Caus, Y. Chabry, J. Nader, J.F. Fusellier, J.L. De Brux, Trends in SAVR with biological vs. mechanical valves in middle-aged patients: results from a French large multi-centric survey, Front. Cardiovasc. Med. 10 (2023) 1205770.

[4] W.C. Frankel, T.C. Nguyen, Artificial heart valves, JAMA 325 (24) (2021) 2512.

[5] C.Y. Chen, C.P. Lin, K.C. Hung, Y.H. Chan, V.C. Wu, Y.T. Cheng, J.K. Yeh, P.H. Chu, A.H. Chou, S.W. Chen, Durability of biological valves implanted in aortic or mitral positions: a nationwide cohort study, Ann. Thorac. Surg. 116 (4) (2023) 751–757.

[6] T. Senage, A. Paul, T. Le Tourneau, I. Fellah-Hebia, M. Vadori, S. Bashir, M. Galiñanes, T. Bottio, G. Gerosa, A. Evangelista, L.P. Badano, A. Nassi, C. Costa, G. Cesare, R.A. Manji, C. Cueff de Monchy, N. Piriou, R. Capoulade, J.M. Serfaty, G. Guimbretière, E. Dantan, A. Ruiz-Majoral, G. Coste du Fou, S. Leviatan Ben-Arye, L. Govani, S. Yehuda, S. Bachar Abramovitch, R. Amon, E.M. Reuven, Y. Atiya-Nasagi, H. Yu, L. Iop, K. Casós, S.G. Kuguel, A. Blasco-Lucas, E. Permanyer, F. Sbraga, R. Llatjós, G. Moreno-Gonzalez, M. Sánchez-Martínez, M.E. Breimer, J. Holgersson, S. Teneberg, M. Pascual-Gilabert, A. Nonell-Canals, Y. Takeuchi, X. Chen, R. Mañez, J.C. Roussel, J.P. Soulillou, E. Cozzi, V. Padler-Karavani, The role of antibody responses against glycans in bioprosthetic heart valve calcification and deterioration, Nat. Med. 28 (2) (2022) 283–294.

[7] R.A. Manji, L.F. Zhu, N.K. Nijjar, D.C. Rayner, G.S. Korbutt, T.A. Churchill, R. V. Rajotte, A. Koshal, D.B. Ross, Glutaraldehyde-fixed bioprosthetic heart valve conduits calcify and fail from xenograft rejection, Circulation 114 (4) (2006) 318–327.

[8] N.R. Nichay, A.A. Dokuchaeva, Y.Y. Kulyabin, E.V. Boyarkin, E.V. Kuznetsova, Y. L. Rusakova, I.S. Murashov, A.A. Vaver, A.V. Bogachev-Prokophiev, I. Y. Zhuravleva, Epoxy- versus glutaraldehyde-treated bovine jugular vein conduit for pulmonary valve replacement: a comparison of morphological changes in a pig model, Biomedicines 11 (11) (2023).

[9] S.M. Zhang, C. Zheng, M.L. Li, K.L. Ding, X.Y. Huang, X.Y. Liang, Y. Lei, Q. Jiang, Y. B. Wang, Sodium lignosulfonate cross-linked bioprosthetic heart valve materials for enhanced cytocompatibility, improved hemocompatibility, and reduced calcification, Compos. Pt. B-Eng. 234 (2022) 11.

[10] A. Shavandi, A.E.A. Bekhit, P. Saeedi, Z. Izadifar, A.A. Bekhit, A. Khademhosseini, Polyphenol uses in biomaterials engineering, Biomaterials 167 (2018) 91–106.

[11] M.J. Wissink, R. Beernink, J.S. Pieper, A.A. Poot, G.H. Engbers, T. Beugeling, W. G. van Aken, J. Feijen, Immobilization of heparin to EDC/NHS-crosslinked collagen. Characterization and in vitro evaluation, Biomaterials 22 (2) (2001) 151–163.

[12] Y. Wu, X. Chen, P. Song, R. Li, Y. Zhou, Q. Wang, J. Shi, W. Qiao, N. Dong, Functional oxidized hyaluronic acid cross-linked decellularized heart valves for improved immunomodulation, anti-calcification, and recellularization, Adv. Healthcare Mater. 13 (16) (2024) e2303737.

[13] G. De Visscher, I. Vranken, A. Lebacq, C. Van Kerrebroeck, J. Ganame, E. Verbeken, W. Flameng, In vivo cellularization of a cross-linked matrix by intraperitoneal implantation: a new tool in heart valve tissue engineering, Eur. Heart J. 28 (11) (2007) 1389–1396.

[14] C. Liu, W. Qiao, H. Cao, J. Dai, F. Li, J. Shi, N. Dong, A riboflavin-ultraviolet light A-crosslinked decellularized heart valve for improved biomechanical properties, stability, and biocompatibility, Biomater. Sci. 8 (9) (2020) 2549–2563.

[15] H. Ghanbari, A. de Mel, A.M. Seifalian, Cardiovascular application of polyhedral oligomeric silsesquioxane nanomaterials: a glimpse into prospective horizons, Int. J. Nanomed. 6 (2011) 775–786.

[16] P. Loman-Cortes, T. Binte Huq, J.L. Vivero-Escoto, Use of polyhedral oligomeric silsesquioxane (POSS) in drug delivery, photodynamic therapy and bioimaging, Molecules 26 (21) (2021).

[17] R.Y. Kannan, H.J. Salacinski, K.M. Sales, P.E. Butler, A.M. Seifalian, The endothelialization of polyhedral oligomeric silsesquioxane nanocomposites: an in vitro study, Cell Biochem. Biophys. 45 (2) (2006) 129–136.

[18] R.Y. Kannan, H.J. Salacinski, J.E. Ghanavi, A. Narula, M. Odlyha, H. Peirovi, P. E. Butler, A.M. Seifalian, Silsesquioxane nanocomposites as tissue implants, Plast. Reconstr. Surg. 119 (6) (2007) 1653–1662.

[19] R.Y. Kannan, H.J. Salacinski, J. De Groot, I. Clatworthy, L. Bozec, M. Horton, P. E. Butler, A.M. Seifalian, The antithrombogenic potential of a polyhedral oligomeric silsesquioxane (POSS) nanocomposite, Biomacromolecules 7 (1) (2006) 215–223.

[20] A.G. Kidane, G. Burriesci, M. Edirisinghe, H. Ghanbari, P. Bonhoeffer, A. M. Seifalian, A novel nanocomposite polymer for development of synthetic heart valve leaflets, Acta Biomater. 5 (7) (2009) 2409–2417.

[21] H. Ghanbari, A.G. Kidane, G. Burriesci, B. Ramesh, A. Darbyshire, A.M. Seifalian, The anti-calcification potential of a silsesquioxane nanocomposite polymer under in vitro conditions: potential material for synthetic leaflet heart valve, Acta Biomater. 6 (11) (2010) 4249–4260.

[22] A. D'Souza A, R. Shegokar, Polyethylene glycol (PEG): a versatile polymer for pharmaceutical applications, Expet Opin. Drug Deliv. 13 (9) (2016) 1257–1275.

[23] M. Ibrahim, E. Ramadan, N.E. Elsadek, S.E. Emam, T. Shimizu, H. Ando, Y. Ishima, O.H. Elgarhy, H.A. Sarhan, A.K. Hussein, T. Ishida, Polyethylene glycol (PEG): the nature, immunogenicity, and role in the hypersensitivity of PEGylated products, J. Contr. Release 351 (2022) 215–230.

[24] D. Ezhilarasan, K.S. Harini, Nanodrug delivery: strategies to circumvent nanoparticle trafficking by Kupffer cells in the liver, J. Drug Deliv. Sci. Technol. 86 (2023) 11.

[25] R. Guo, Y. Zhou, S. Liu, C. Li, C. Lu, G. Yang, J. Nie, F. Wang, N.G. Dong, J. Shi, Anticalcification potential of POSS-PEG hybrid hydrogel as a scaffold material for the development of synthetic heart valve leaflets, ACS Appl. Bio Mater. 4 (3) (2021) 2534–2543.

[26] C. Li, Y. Zhou, S. Liu, R. Guo, C. Lu, D. Yin, Y. Zhang, X. Xu, N. Dong, J. Shi, Surface modification of decellularized heart valve by the POSS-PEG hybrid hydrogel to prepare a composite scaffold material with anticalcification potential, ACS Appl. Bio Mater. 5 (8) (2022) 3923–3935.

[27] C. Zhou, T. Jiang, S. Liu, Y. He, G. Yang, J. Nie, F. Wang, X. Yang, Z. Chen, C. Lu, AgNPs loaded adenine-modified chitosan composite POSS-PEG hybrid hydrogel with enhanced antibacterial and cell proliferation properties for promotion of infected wound healing, Int. J. Biol. Macromol. 267 (Pt 1) (2024) 131575.

[28] C. Li, T. Jiang, C. Zhou, A. Jiang, C. Lu, G. Yang, J. Nie, F. Wang, X. Yang, Z. Chen, Injectable self-healing chitosan-based POSS-PEG hybrid hydrogel as wound dressing to promote diabetic wound healing, Carbohydr. Polym. 299 (2023) 120198.

[29] M. Xie, J. Ge, B. Lei, Q. Zhang, X. Chen, P.X. Ma, Star-shaped, biodegradable, and elastomeric PLLA-PEG-POSS hybrid membrane with biomineralization activity for guiding bone tissue regeneration, Macromol. Biosci. 15 (12) (2015) 1656–1662.

[30] K. Findeisen, L. Morticelli, T. Goecke, L. Kolbeck, R. Ramm, H.K. Höffler, G. Brandes, S. Korossis, A. Haverich, A. Hilfiker, Toward acellular xenogeneic heart valve prostheses: histological and biomechanical characterization of decellularized and enzymatically deglycosylated porcine pulmonary heart valve matrices, Xenotransplantation 27 (5) (2020) e12617.

[31] Y. Snyder, S. Jana, Strategies for development of decellularized heart valve scaffolds for tissue engineering, Biomaterials 288 (2022) 121675.

[32] J. Li, W. Qiao, Y. Liu, H. Lei, S. Wang, Y. Xu, Y. Zhou, S. Wen, Z. Yang, W. Wan, J. Shi, N. Dong, Y. Wu, Facile engineering of interactive double network hydrogels for heart valve regeneration, Nat. Commun. 15 (1) (2024) 7462.

[33] M. Hu, S. Shi, X. Peng, X. Pu, X. Yu, A synergistic strategy of dual-crosslinking and loading intelligent nanogels for enhancing anti-coagulation, pro-endothelialization and anti-calcification properties in bioprosthetic heart valves, Acta Biomater. 171 (2023) 466–481.

[34] W.K. Loke, E. Khor, Validation of the shrinkage temperature of animal tissue for bioprosthetic heart valve application by differential scanning calorimetry, Biomaterials 16 (3) (1995) 251–258.

[35] I.H. Jaffer, J.C. Fredenburgh, J. Hirsh, J.I. Weitz, Medical device-induced thrombosis: what causes it and how can we prevent it? J. Thromb. Haemostasis 13 (Suppl 1) (2015) S72–S81.

[36] J.H. Lee, H.B. Lee, Platelet adhesion onto wettability gradient surfaces in the absence and presence of plasma proteins, J. Biomed. Mater. Res. 41 (2) (1998) 304–311.

[37] N. Yayapour, H. Nygren, Interactions between whole blood and hydrophilic or hydrophobic glass surfaces: kinetics of cell adhesion, Colloids Surf. B Biointerfaces 15 (2) (1999) 127–138.

[38] M. Rahmati, E.A. Silva, J.E. Reseland, A. H C, H.J. Haugen, Biological responses to physicochemical properties of biomaterial surface, Chem. Soc. Rev. 49 (15) (2020) 5178–5224.

[39] S.A. Skoog, G. Kumar, R.J. Narayan, P.L. Goering, Biological responses to immobilized microscale and nanoscale surface topographies, Pharmacol. Ther. 182 (2018) 33–55.

[40] J.G. McCarron, M.D. Lee, C. Wilson, The endothelium solves problems that endothelial cells do not know exist, Trends Pharmacol. Sci. 38 (4) (2017) 322–338.

[41] B.P. Reines, B.W. Ninham, Structure and function of the endothelial surface layer: unraveling the nanoarchitecture of biological surfaces, Q. Rev. Biophys. 52 (2019) e13.

[42] T. Yu, G. Li, X. Chen, D. Kuang, Q. Jiang, Y. Guo, Y. Wang, A versatile drug-controlled release polymer brush hybrid non-glutaraldehyde bioprosthetic heart valves with enhanced anti-inflammatory, anticoagulant and anti-calcification properties, and superior mechanical performance, Biomaterials 296 (2023) 122070.

[43] Y. Zhang, H. Hu, Y. Zhu, J. Xiao, C. Li, C. Qian, X. Yu, J. Zhao, X. Chen, J. Liu, J. Zhou, Butterfly-inspired multiple cross-linked dopamine-metal-phenol bioprosthetic valves with enhanced endothelialization and anticalcification, ACS Appl. Mater. Interfaces 16 (47) (2024) 64522–64535.

[44] J.H. Pang, Y. Farhatnia, F. Godarzi, A. Tan, J. Rajadas, B.G. Cousins, A.M. Seifalian, In situ endothelialization: bioengineering considerations to translation, Small 11 (47) (2015) 6248–6264.

[45] S. Jana, Endothelialization of cardiovascular devices, Acta Biomater. 99 (2019) 53–71.

[46] T. Yu, C. Zheng, X. Chen, H. Pu, G. Li, Q. Jiang, Y. Wang, Y. Guo, A universal strategy for the construction of polymer brush hybrid non-glutaraldehyde heart valves with robust anti-biological contamination performance and improved endothelialization potential, Acta Biomater. 160 (2023) 87–97.

[47] G.D. Dangas, J.I. Weitz, G. Giustino, R. Makkar, R. Mehran, Prosthetic heart valve thrombosis, J. Am. Coll. Cardiol. 68 (24) (2016) 2670–2689.

[48] T.R.G. Cartlidge, M.K. Doris, S.L. Sellers, T.A. Pawade, A.C. White, R. Pessotto, J. Kwiecinski, A. Fletcher, C. Alcaide, C. Lucatelli, C. Densem, J.H.F. Rudd, E.J. R. van Beek, A. Tavares, R. Virmani, D. Berman, J.A. Leipsic, D.E. Newby, M. R. Dweck, Detection and prediction of bioprosthetic aortic valve degeneration, J. Am. Coll. Cardiol. 73 (10) (2019) 1107–1119.

[49] G. Yan, M. Fan, Y. Zhou, M. Xie, J. Shi, N. Dong, Q. Wang, W. Qiao, Chondroitin sulfate derivative cross-linking of decellularized heart valve for the improvement

of mechanical properties, hemocompatibility, and endothelialization, ACS Appl. Mater. Interfaces 16 (28) (2024) 35936–35948.
[50] S.F. Saleeb, J.W. Newburger, T. Geva, C.W. Baird, K. Gauvreau, R.F. Padera, P. J. Del Nido, M.J. Borisuk, S.P. Sanders, J.E. Mayer, Accelerated degeneration of a bovine pericardial bioprosthetic aortic valve in children and young adults, Circulation 130 (1) (2014) 51–60.
[51] S. Xue, Z. Su, D. Liu, Immunometabolism and immune response regulate macrophage function in atherosclerosis, Ageing Res. Rev. 90 (2023) 101993.
[52] B.V. Kumar, T.J. Connors, D.L. Farber, Human T cell development, localization, and function throughout Life, Immunity 48 (2) (2018) 202–213.
[53] V. Penugurti, R.K. Manne, L. Bai, R. Kant, H.K. Lin, AMPK: the energy sensor at the crossroads of aging and cancer, Semin. Cancer Biol. 106–107 (2024) 15–27.
[54] N. Wang, B. Wang, E.P. Maswikiti, Y. Yu, K. Song, C. Ma, X. Han, H. Ma, X. Deng, R. Yu, H. Chen, AMPK-a key factor in crosstalk between tumor cell energy metabolism and immune microenvironment? Cell Death Dis. 10 (1) (2024) 237.
[55] L. Huangfu, R. Li, Y. Huang, S. Wang, The IL-17 family in diseases: from bench to bedside, Signal Transduct. Targeted Ther. 8 (1) (2023) 402.
[56] X. Li, R. Bechara, J. Zhao, M.J. McGeachy, S.L. Gaffen, IL-17 receptor-based signaling and implications for disease, Nat. Immunol. 20 (12) (2019) 1594–1602.
[57] H. Pu, C. Wang, T. Yu, X. Chen, G. Li, D. Zhu, X. Pan, Y. Wang, A synergistic strategy based on active hydroxymethyl amine compounds and fucoidan for bioprosthetic heart valves with enhancing anti-coagulation and anti-calcification properties, Int. J. Biol. Macromol. 266 (Pt 2) (2024) 130715.
[58] T. Yu, H. Pu, X. Chen, Q. Kong, C. Chen, G. Li, Q. Jiang, Y. Wang, A versatile modification strategy for functional non-glutaraldehyde cross-linked bioprosthetic heart valves with enhanced anticoagulant, anticalcification and endothelialization properties, Acta Biomater. 160 (2023) 45–58.
[59] M. Hu, X. Peng, S. Shi, C. Wan, C. Cheng, X. Yu, Dialdehyde xanthan gum and curcumin synergistically crosslinked bioprosthetic valve leaflets with anti-thrombotic, anti-inflammatory and anti-calcification properties, Carbohydr. Polym. 310 (2023) 120724.
[60] S. Wen, Y. Zhou, W.Y. Yim, S. Wang, L. Xu, J. Shi, W. Qiao, N. Dong, Mechanisms and drug therapies of bioprosthetic heart valve calcification, Front. Pharmacol. 13 (2022) 909801.